NANO LETTERS

2006
Vol. 6, No. 8
1794−1807

Comparison of the Abilities of Ambient and Manufactured Nanoparticles To Induce Cellular Toxicity According to an Oxidative Stress Paradigm

Tian Xia,[†,‡] Michael Kovochich,[†,‡] Jonathan Brant,[§] Matt Hotze,[§] Joan Sempf,[||] Terry Oberley,[||] Constantinos Sioutas,[⊥,#] Joanne I. Yeh,[+] Mark R. Wiesner,[§] and Andre E. Nel*[,†,#]

Division of Clinical Immunology and Allergy, Department of Medicine, University of California, Los Angeles, California 90095, Department of Civil & Environmental Engineering, Duke University, Durham, North Carolina 27708, Pathology Service, Veterans Administration Medical Center, Madison, Wisconsin 53792, Department of Civil and Environmental Engineering, University of Southern California, Los Angeles, California 90089, The Southern California Particle Center, University of California, Los Angeles, California 90095, and Department of Structural Biology, Department of Bioengineering, University of Pittsburgh School of Medicine, Pittsburgh, Pennsylvania 15260

Received May 5, 2006; Revised Manuscript Received June 20, 2006

ABSTRACT

Nanomaterial properties differ from those bulk materials of the same composition, allowing them to execute novel activities. A possible downside of these capabilities is harmful interactions with biological systems, with the potential to generate toxicity. An approach to assess the safety of nanomaterials is urgently required. We compared the cellular effects of ambient ultrafine particles with manufactured titanium dioxide (TiO_2), carbon black, fullerol, and polystyrene (PS) nanoparticles (NPs). The study was conducted in a phagocytic cell line (RAW 264.7) that is representative of a lung target for NPs. Physicochemical characterization of the NPs showed a dramatic change in their state of aggregation, dispersibility, and charge during transfer from a buffered aqueous solution to cell culture medium. Particles differed with respect to cellular uptake, subcellular localization, and ability to catalyze the production of reactive oxygen species (ROS) under biotic and abiotic conditions. Spontaneous ROS production was compared by using an ROS quencher (furfuryl alcohol) as well as an NADPH peroxidase bioelectrode platform. Among the particles tested, ambient ultrafine particles (UFPs) and cationic PS nanospheres were capable of inducing cellular ROS production, GSH depletion, and toxic oxidative stress. This toxicity involves mitochondrial injury through increased calcium uptake and structural organellar damage. Although active under abiotic conditions, TiO_2 and fullerol did not induce toxic oxidative stress. While increased TNF-α production could be seen to accompany UFP-induced oxidant injury, cationic PS nanospheres induced mitochondrial damage and cell death without inflammation. In summary, we demonstrate that ROS generation and oxidative stress are a valid test paradigm to compare NP toxicity. Although not all materials have electronic configurations or surface properties to allow spontaneous ROS generation, particle interactions with cellular components are capable of generating oxidative stress.

Introduction. The unique physicochemical properties of engineered nanoparticles (NPs) are attributable to their small size, large surface area, chemical composition, surface reactivity, charge, shape, and media interactions.[1−4] Although impressive from the perspective of material science, the novel properties of NPs could lead to adverse biological effects, with the potential to create toxicity. Indeed, some studies have shown that NPs could exert toxic effects and pose hazards to humans and the environment.[1−4] Nanotoxicology is an emerging science that demands an understanding of the physicochemical properties of nanomaterials that may lead to adverse biological outcomes.

While the extraordinary properties of nanomaterials could necessitate a novel investigative approach, research into air

*Corresponding author: Department of Medicine, Division of Clinical Immunology & Allergy, UCLA School of Medicine, 52-175 CHS, 10833 Le Conte Ave, Los Angeles, CA 90095-1680. Tel: (310) 825-6620. Fax: (310) 206-8107. E-mail: anel@mednet.ucla.edu.

[†] Division of Clinical Immunology and Allergy, Department of Medicine, University of California.

[‡] Contributed equally to this work.

[§] Department of Civil & Environmental Engineering, Duke University.

[||] Pathology Service, Veterans Administration Medical Center.

[⊥] Department of Civil and Environmental Engineering, University of Southern California.

[#] The Southern California Particle Center, University of California.

[+] Department of Structural Biology, Department of Bioengineering, University of Pittsburgh School of Medicine.

10.1021/nl061025k CCC: $33.50
Published on Web 07/26/2006

pollution and mineral dust particles has established a scientific basis for assessing lung and cardiovascular injury by inhaled particles.[3−5] This includes evidence that ambient ultrafine particles (particulate matter with physical diameters <100 nm) induce reactive oxygen species (ROS), oxidative stress, and inflammation in the lung and vasculature. Likewise, occupational exposure to quartz and mineral dust particles (e.g., coal and silicates) could induce oxidative injury, inflammation, fibrosis, and cytotoxicity in the lung.[3−7] Tissue and cell culture analyses support the in vivo outcomes, pointing to the role of ROS and oxidative stress in the generation of proinflammatory responses and cytotoxic effects. Taken together, these clinical and experimental studies indicate that a small size, large surface area, chemical composition, and ability to generate ROS play a key role in the ability of ambient NP to induce lung injury.[3−7]

Although the heterogeneous characteristics of ambient ultrafine particles (UFPs) are very different from the homogeneous composition of manufactured NPs, the limited data on manufactured particles indicate that ROS production could also feature as a mechanism of toxicity. For instance, water-soluble fullerenes induce $O_2^{\bullet-}$ anions, lipid peroxidation, and cytotoxicity.[8] ROS production, lipid peroxidation, and the generation of proinflammatory responses have also been described in tissue culture and animal studies that addressed the potential toxicity of metal oxide particles (e.g., TiO_2) and carbon nanotubes.[9−12] This suggests that an investigation into the mechanisms of ROS production and their biological consequences could serve as a paradigm for NP toxicity.

Oxidative stress is a state of redox disequilibrium in which ROS production overwhelms the antioxidant defense capacity of the cell, thereby leading to adverse biological consequences. Oxidative stress is often expressed in terms of the glutathione (GSH) to glutathione disulfide (GSSG) ratio in the cell.[13] The GSH/GSSG redox couple not only serves as the chief homeostatic regulator of cellular redox balance but also functions as a sensor that triggers cellular responses, which, depending on the rate and level of decline, could be protective or injurious in nature.[7,13−15] The hierarchical oxidative stress model posits that minor levels of oxidative stress induce protective effects that may yield to more damaging effects at higher levels of oxidative stress. The protective cellular effects are regulated by the transcription factor, nuclear factor, erythroid 2-related factor 2 (Nrf2), which leads to transcriptional activation of >200 antioxidant and detoxification enzymes that are collectively known as the phase II response. Examples of phase II enzymes include heme oxygenase 1 (HO-1), glutathione-S-transferase (GST) isoenzymes, NADPH quinone oxidoreductase (NQO1), catalase, superoxide dismutase, and glutathione peroxidase (GPx).[16,17] Defects or aberrancy of this protective pathway could determine the susceptibility to particle-induced oxidant injury, e.g., the exacerbation of allergic inflammation and asthma by exposure to diesel exhaust particles (DEPs).[17] Should these protective responses fail to provide adequate protection, a further increase in ROS production can result in proinflammatory and cytotoxic effects. Proinflammatory effects are mediated by the redox-sensitive MAP kinase and NF-κB cascades that lead to the expression of cytokines, chemokines, and adhesion molecules.[15−18] In contrast, cytotoxic effects are mediated by mitochondria, which are capable of releasing pro-apoptotic factors. It is noteworthy that several types of NPs have the capacity to target mitochondria directly.[3,15]

Despite the intense interest in nanomaterial safety, no comprehensive test paradigm has been developed to compare the toxicity of different nanomaterials. However, some of the procedures and assays that have been developed to assess the adverse biological effects of ambient PM could be helpful to study manufactured NPs. In particular, the ability to generate ROS and oxidant injury may provide a paradigm to compare the toxic potential of NPs. In this communication, we will compare a number of manufactured NPs with ambient UFPs to determine whether this is a valid paradigm for NP toxicity. We demonstrate that ROS generation and mitochondrial injury constitute quantifiable toxicological responses for ambient UFPs and cationic polystyrene nanospheres. We also demonstrate that the physicochemical properties of the particles, particularly chemical composition, charge, and size determine the capability toward ROS generation under abiotic and biotic conditions.

Materials and Methods. A detailed description of the materials and methods used in this study appear in Supporting Information. Ambient UFPs (<0.1 μm) were collected in the Los Angeles basin through the use of particle concentrator technology as described by us.[19] Carbon black (CB) (Printex 90) and titanium dioxide (P25) NPs were obtained from Degussa (Hanau, Germany). Fullerol was from MER Corp. (Tucson, AZ). Polystyrene (PS) nanospheres were obtained from Bangs Laboratory (Fishers, IN). The chemical characterization of these particles as well as assessment of particle size, shape, state of aggregation, charge, hydrophilicity/hydrophobicity, and ability to generate ROS under abiotic conditions are described in the Supporting Information. The assessment of ROS production under biotic and abiotic conditions, heme-oxygenase 1 (HO-1) expression, Jun kinase activation, TNF-α production, mitochondrial membrane potential, and cellular ultrastructure also appears in the Supporting Information. Cellular assays were carried out in a murine macrophage cell line, RAW 264.7. Cell culture conditions and a description of the biological assays are described in Supporting Information. NP exposures were conducted by incubating triplicate aliquots of 3×10^5 RAW 264.7 cells in 24-well plates. Each well received 500 μL of complete medium (DMEM) that includes 10% fetal calf serum (FCS) and antibiotics. All NP suspensions were prepared fresh from a stock solution as described in the Supporting Information. Results were analyzed by the Student's *t* test unless otherwise specified, and expressed as the mean ± standard deviation.

Results. (A) Particle Selection and Physical−Chemical Characterization. The particles that are being compared in this study are listed in Table 1 and their corresponding transmission electron microscopy (TEM) images are shown in Figure 1. Ambient UFPs were chosen as a NP source that

Table 1. Physical Characterization of Nanoparticles[a]

particle	av diameter (nm)	PDI	electrophoretic mobility U (μm cm/(V s))	zeta potential ζ (mV)	MATH (%)
			In Aqueous Media		
UFP	1034	1.0	−2.28	−29.1	8.2
PS	68	0.041	−2.85	−36.4	2.7
NH_2-$PS_{60\ nm}$	65	0.055	3.15	40.3	5.3
NH_2-$PS_{600\ nm}$	648	0.096	3.58	45.8	4.2
COOH-PS	56	0.063	−2.15	−27.6	0.0
TiO_2	364	0.466	−1.28	−16.4	1.6
carbon black	245	0.251	−4.26	−54.6	7.1
fullerol	218	0.388	−1.76	−22.6	0.6
			In Cell Culture Medium		
UFP	1778	0.379	−0.86	−11.0	
PS	90	0.200	−1.00	−12.7	
NH_2-$PS_{60\ nm}$	527	0.339	−0.87	−11.1	
NH_2-$PS_{600\ nm}$	1913	1.0	−0.96	−12.2	
COOH-PS	82	0.191	−0.85	−10.9	
TiO_2	175	0.877	−0.97	−12.4	
carbon black	154	0.278	−1.06	−13.5	
fullerol	106	0.700	−0.97	−12.4	

[a] The reported mean particle size (average diameter) is calculated based on an intensity weighted average; PDI = polydispersity index; MATH = microbial adhesion to hydrocarbon test.

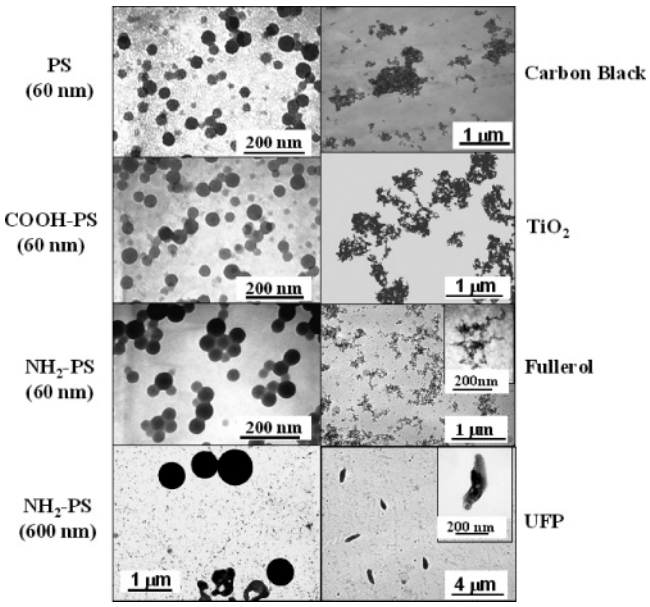

Figure 1. TEM of the NPs used in this study. All NPs were prepared into solution and applied to a grid as described in the Supporting Information. Pictures were taken with Hitachi electron microscope (Hitachi Instrument Inc., Tokyo, Japan).

exhibit known health risks and have a defined mechanism of biological injury, namely, ROS generation.[19,20] These particles were collected in downtown Los Angeles by means of the versatile aerosol concentration enrichment system (VACES).[19,21] Atmospheric UFPs have a mean aerodynamic diameter of 30 nm (Figure S1, Supporting Information). However, combustion-generated particles have the tendency to grow from nearly spherical primary particles into fractal-like agglomerates with high carbon content. Diesel engines, in particular, emit large amounts of agglomerate soot particles.[22,23] To conduct biological experiments, the effluent line of the VACES was connected to a liquid impinger, which allows the supersaturated UFPs to be collected as water droplets. When suspended in water, the UFP agglomerates form fractal structures (Figure 1).

UFPs generate ROS and oxidative stress based on their content of organic chemicals and transition metals.[19,20] These reactions could take place on the particle surface or the surrounding aqueous medium after leaching of the chemicals from the particle surface. The complete chemical characterization of these particles is shown in Supporting Information (Figure S1B). A noteworthy class of components in the organic fraction is polycyclic aromatic hydrocarbons (PAHs) (Figure S1B), including functionalized derivatives such as quinones.[24] A graphical display of UFP size distribution in aqueous buffer and the culture medium environments appear in the Supporting Information (Figure S1A). Compared to other particle types, UFPs exhibit a high polydispersity index (PDI) (Table 1). These particles are negatively charged in the aqueous buffer as determined by their isoelectrophoretic mobility and zeta potential (Table 1). Due to their coating with organic chemicals, UFPs exhibit a relatively high hydrophobicity index, as determined by the microbial adhesion to hydrocarbon (MATH) test (Table 1). The MATH assay assesses NP partitioning between laboratory grade *n*-dodecane and water (Supporting Information). The relatively high hydrophobicity index of these particles could be important for their cellular uptake, as will be discussed later.

Carbon black (CB) nanoparticles (Printex 90) were included as a control for the UFPs. Although these particles have a carbon backbone, they exhibit a low PAH content and no measurable transition metals (Table S1). Since CB nanoparticles are produced in bulk, are in widespread use, and could be spread via the air, they are indeed important NPs from a toxicological perspective. These particles have a BET surface area of 300 m^2/g with a mean primary particle diameter of 14 nm.[25] Printex 90 particles exhibit a considerable tendency to aggregate in aqueous medium (Figure 1), although not to the same degree as UFPs. Their PDI = 0.25, and they exhibit a relatively high hydrophobicity index (Table 1). These particles carry a negative charge (Table 1).

TiO_2 is another NP type that is produced in millions of tons per year and is used in a wide range of consumer products. The P25 particles from Degussa contains 80% anatase and 20% rutile (Table S1). They have a BET surface area of 50 m^2/g, and a primary particle diameter of 20−30 nm.[26] TiO_2 is capable of spontaneous ROS production, as will be discussed later. These particles form large aggregates with a PDI of 0.45 (Figure 1, Table 1). They carry a negative surface charge and exhibit a relatively low hydrophobicity index (Table 1).

Fullerol is a hydroxylated C_{60} ($C_{60}(OH)_m$, $m = 22-26$) fullerene derivative that is capable of ROS production under abiotic conditions but requires an appropriate electron donor to do so.[27] Various forms of fullerenes are emerging as additives to consumer products such as cosmetics, tires, batteries, and tennis rackets. Fullerol forms large aggregates with a PDI = 0.39, a negative zeta potential, and a relatively low hydrophobicity index (Figure 1, Table 1).

In contrast to other engineered NPs, polystyrene (PS) nanospheres remain monodisperse (PDI < 0.1) under aque-

ous aqueous conditions (Figure 1, Table 1). PS particles are available in a variety of sizes and can also be purchased as positively charged amino (NH_2)-PS or negatively charged carboxylated (COOH)-PS nanospheres. This allows an independent assessment of the role of particle size and charge by a material that lacks semiconductor capabilities and is incapable of ROS generation. Physical−chemical analysis reveals that 60 and 600 nm NH_2-labeled PS spheres indeed exhibit a positive zeta potential, while that of the 60 nm neutral and COOH−PS nanospheres were negative (Table 1). All PS nanospheres are relatively hydrophobic except for the COOH−PS particles that are more hydrophilic (Table 1).

NP characteristics were also assessed in complete culture medium (that includes DMEM and 10% FCS). In the presence of complete medium, NH_2−PS particles show a considerable increase in size due to agglomeration, while other NPs showed smaller increases or no changes (Table 1, Figures S2 and S3). Accordingly, the PDI of NH_2−PS particles increased substantially (Table 1). A possible explanation is that proteins in the culture media may be adsorbed onto the particle surface, leading to neutralization of charge and interference in electrostatic repulsion. This notion is supported by the near-equalization of the zeta potential of the particles (Table 1, bottom panel).

(B) Assessment of ROS Generation and Speciation under Abiotic Conditions. A number of studies indicate that some NP exhibits the potential for spontaneous ROS generation based on material composition and surface characteristics. Examples include the presence of redox-cycling chemicals (UFP), crystallinity of the material surface and electronic configurations (TiO_2), UV excitability (TiO_2 and fullerol), and presence of a conjugated π-bond system (fullerol). We used two complementary techniques to assess ROS generation by the NP. The first uses the ROS quencher, furfuryl alcohol (FFA), to measure the rate of oxygen consumption as an indirect indicator of the amounts that are being produced.[28] Because FFA quenches ROS production, the quantity of ROS that is being produced is measured as a decrease in dissolved oxygen, corrected for the appropriate blank. Results from the indirect measurements are plotted as the log of the ratio of the instantaneous to initial concentrations of oxygen measured over time (Figure 2). A steeper slope corresponds to a higher rate of ROS production. The TiO_2 nanoparticles displayed the highest rate of ROS production under UV irradiation, followed closely by fullerol. This result is particularly significant given the recognized efficiency of TiO_2 as a photocatalyst. While hydroxylation of the C_{60} cage is thought to reduce the net generation of singlet oxygen compared with the nonderivatized molecule,[29,30] fullerol nonetheless appears to be a relatively powerful ROS producer. UFPs also produced significant quantities of ROS, in contrast with the polystyrene particles that were inert (Figure 2). A lack of ROS production by the PS particles is expected, as these particles are neither semiconductors nor photosensitizers. Although FFA does not differentiate between different ROS, supplementary techniques such as the use of electron spin trapping and quenchers such as superoxide dismutase (SOD) suggest that this assay measures multiple species.

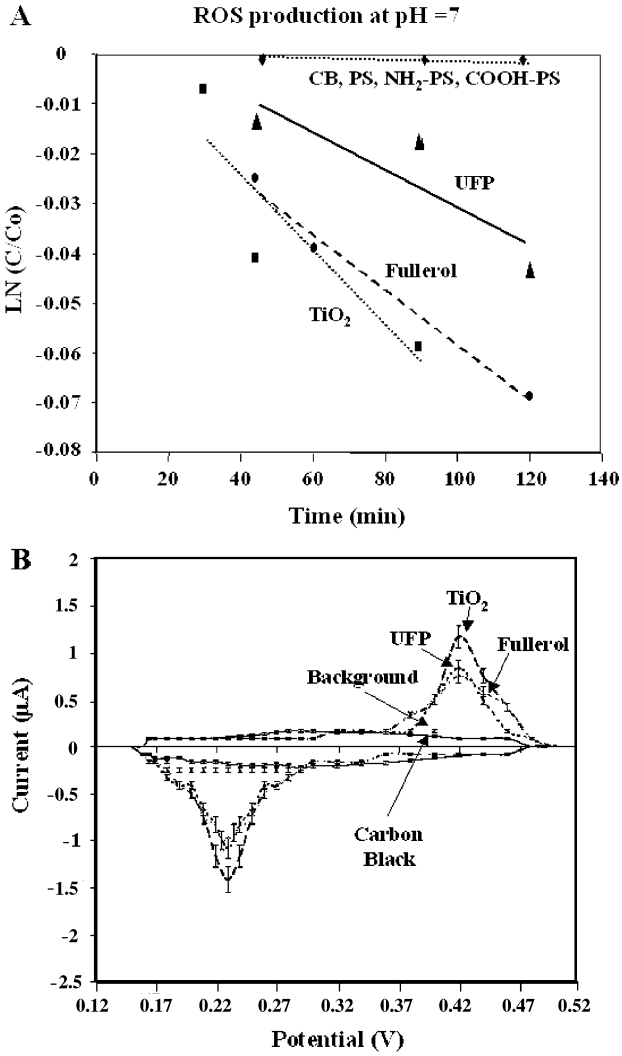

Figure 2. The ROS generating capacity of NPs under abiotic conditions was performed as described in the Supporting Information: (A) FFA assay, 0.5 mg/L nanoparticles were added to a solution of 100 mM furfuryl alcohol in aerated phosphate buffer (pH=7); (B) CNT-Npx-bioelectrode platform, cyclic voltammograms of individual NP demonstrate a clear redox signal for UFPs, TiO_2, and fullerol, whereas CB was inactive. The negative CB profile also represents similar results obtained with all the PS nanospheres (not shown).

Because the FFA assay does not assess speciation, we exploited the efficiency and specificity of redox enzymes to develop a nano-biosensor that is relatively specific for H_2O_2.[31,32] It has been reported recently that carbon nanotubes (CNTs) can be used to promote direct electron transfer from redox enzymes to an electrode surface.[33] Details about the assembly of this electrode and its use are described in the Supplementary Information section, along with pictorial displays of the bioelectrode and its assembly (Figure S4A−C). Introduction of NPs to the CNT-Npx-bioelectrode array demonstrated H_2O_2 generation by UFPs, TiO_2, and fullerol samples (Figure 2). Similar to the FFA assay, TiO_2 generated the strongest signal, followed by UFPs, and then fullerol (Figure 2). In contrast, CB and PS nanospheres showed little

Table 2. Time-Dependent H_2O_2 Production As Assessed by the Nanobiosensor[a]

nanomaterial	day 0	day 1	day 3	day 7	day 12	day 21
UFP	++	++	++	++	+	−
TiO_2	+++	+++	++	++	+	+
fullerol	++	++	++	±	−	0
carbon black	0	0	0	0	0	0
PS	±	0	0	0	0	0

[a] In vitro detection of oxidative species in solution. All NPs were prepared at 50 pM in 1 mL of water. The presence of oxidants is detected in the cyclic voltammogram (CV) scans (Figure 2B). The absence of a signal in the carbon black sample demonstrated is in Figure 2B. PS gave a very low signal on day 0, which quickly dropped to baseline. UFPs, TiO_2, and fullerol all gave clear signals that continued for up to about 2 weeks. Legend: +, presence of oxidant, number of plus signs indicates signal strength; ±, indicates decreasing signal for oxidant; −, baseline signal for oxidant; 0, no detectable signal for oxidant.

signal above baseline (CB alone is shown to avoid the data crowding, Figure 2). The longevity of the oxidant signals was followed over 3 weeks (Table 2), with UFP, TiO_2, and fullerol exhibiting the potential for continuous oxidant generation over a time period of at least 7 days. The decrease in the signal strength by day 12 could be due to decreased activity of the enzyme component of the biosensor. Taken together, these data show that some but not all NP are capable of spontaneous ROS generation. A key question is whether this activity is related to biological ROS production and oxidant injury.

(C) Induction of ROS Production in RAW 264.7 Cells. ROS generation by NPs was detected in macrophages by using the fluorescent dyes, dichlorofluorescein diacetate (DCFH-DA) and MitoSOX Red (Figures 3 and 4). In the presence of a H_2O_2 and hydroxyl ($OH^{\bullet}$) radicals, DCFH is oxidatively modified into a highly fluorescent derivative, 2,7-dichlorofluorescein (DCF). DCF fluorescence was detected in RAW 264.7 cells by a flow cytometry procedure, in which the fold-increase in mean fluorescence intensity (MFI) was expressed as the ratio of particle-treated vs control cells (Figure 3A). Increased DCF fluorescence commenced <1 h of the addition of UFP and then continued to increase for 4 h before beginning to decline (Figure 3B). Pretreatment of the cells with the thiol antioxidant, *N*-acetylcysteine (NAC), significantly suppressed H_2O_2 production at 4 and 16 h (Figure 3C). This is in agreement with previous studies showing that the redox cycling organic chemicals that are present on the UFP surface are directly neutralized by NAC.[15,34] NAC also acts as a radical scavenger and precursor of glutathione (GSH) synthesis. In the testing of manufactured NP, only the cationic PS nanospheres induced an effect of similar magnitude ($p < 0.01$) as UFP (Figure 3D). NAC effectively disrupted the ROS production by NH_2−PS particles, suggesting that these particles engage in a thiol-dependent biological reaction (not shown). Fullerol generated a small but statistically significant ($p < 0.05$) increase in DCF fluorescence (Figure 3D).

MitoSOX Red is a novel fluorogenic indicator offering direct measurement of superoxide ($O_2^{\bullet-}$) production in live cells.[35] UFP exposure leads to a significant increase in the percent of bright (M1)-fluorescent cells (Figure 4A), as well as an increase in MFI. This increase commenced <2 h and remained stable for 8 h, whereupon a sudden acceleration in the rate of $O_2^{\bullet-}$ production leads to a progressive increase in fluorescent intensity for up to 16 h (Figure 4C). Compared to UFP, all commercial NPs were inactive except for the NH_2−PS nanospheres (Figure 4B). These nanospheres generated a biphasic ROS response (Figure 4C). The first peak reached its maximum at 5 h, followed by a decline and then a progressive increase >8 h (Figure 4C). Interestingly, NAC could interfere in UFP-induced $O_2^{\bullet-}$ generation at all time points but had different effects on NH_2−PS responses at 8 and 16 h time points (Figures 4D and S5). Thus, while NAC failed to suppress the ROS response at 8 h (not shown), it did interfere in the NH_2−PS response at 16 h (Figures 4D and S5).

All considered, UFPs participate in spontaneous and cell-mediated ROS production. Among the manufactured particles, only fullerol could mimic these actions. Despite being the most active material under abiotic conditions, TiO_2 did not generate ROS in cells. This is diagonally opposite from NH_2−PS nanospheres that are incapable of spontaneous ROS production, yet are potent inducers of H_2O_2 and $O_2^{\bullet-}$ generation at cellular level. A key question therefore becomes whether differences in ROS production at a cellular level translate into different levels of biological injury.

(D) UFP and NH_2-PS Nanospheres Are Capable of Inducing Oxidative Stress As Reflected by GSH Depletion and Heme Oxygenase 1 (HO-1) Expression. Whether a biological response will follow ROS production is dependent on the magnitude of the response as well as the antioxidant defense capability of the cell. The GSH vs the GSSG content of the cell acts as a sensor that elicits further cellular responses. Cellular thiol levels can be assessed with a thiol-interactive fluorescent dye, monobromobimane (MBB). While treatment with UFP and NH_2-PS nanospheres induced a dose-dependent decline in MBB fluorescence, CB, TiO_2, fullerol, and other forms of PS nanospheres had no effect (Figure 5A). The kinetics of the UFPs and NH_2-PS responses differ. While UFPs failed to cause thiol depletion for up to 8 h, NH_2-PS induced a more rapid and linear rate of decline (Figure 5B), suggesting different biological mechanisms of action.

According to the hierarchical oxidative stress hypothesis,[15] cells respond to even minimal levels of oxidative stress with a protective antioxidant response. This pathway is dependent on transcriptional activation of phase II gene promoters by the transcription factor, Nrf2. HO-1 is a prime example of a phase II enzyme that mediates antioxidant, antiinflammatory, and cytoprotective effects and is useful as a marker for particle-induced oxidative stress. Using an immunoblotting approach to assess HO-1 expression, both UFP and NH_2-PS nanospheres could be seen to elicit a response, while fullerol, CB, TiO_2, and other PS nanoparticles were ineffective (Figure 6A,B). The effect of UFPs is dose-dependent (Figure S6A). GAPDH immunoblotting was used to ascertain equal protein loading (lower panels). These data indicate that UFP and NH_2-PS are indeed capable of generating biologically relevant oxidative stress effects. The induction of HO-1

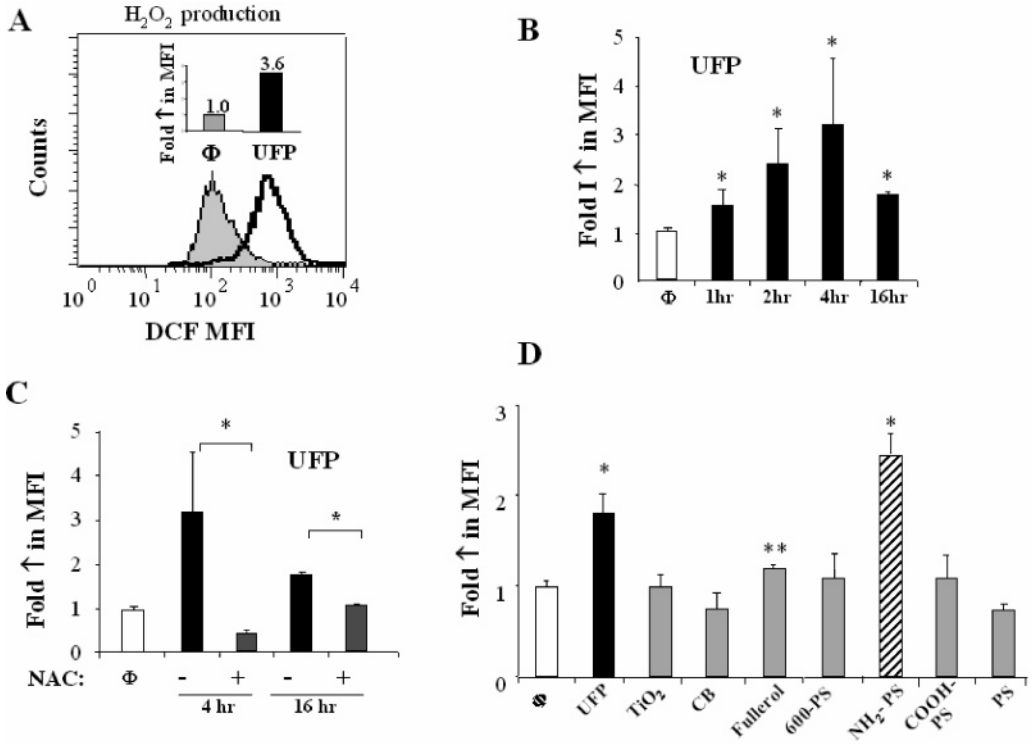

Figure 3. DCF fluorescence in RAW 264.7 cells treated with NPs: (A) histogram to show the fold increase in mean fluorescence intensity (MFI) in RAW 264.7 cells, stained with 2.5 μM DCF-DA, and treated with 10 μg/mL UFP for 4 h; (B) time course of H_2O_2 generation in response to UFP treatment; (C) effect of NAC (10 mM) on UFP-induced H_2O_2 production at 4 and 16 h; (D) comparison of the effect of UFPs, fullerol, CB, TiO_2, and PS particles. All particles were used at 10 μg/mL and used to treat cells for 4 or 16 h. Data are representative of three separate experiments. *$p < 0.01$, compared to control.

expression was suppressed by NAC (Figure 6C). These data demonstrate that some but not all NPs are capable of generating oxidative stress under biological conditions.

(E) Jun Kinase Activation and TNF-α Production as a Reflection of Proinflammatory Responses. When antioxidant defenses fail to restore redox equilibrium, escalation in the level of oxidative stress could lead to cellular injury. One mechanism is the activation of proinflammatory cascades. The Jun kinase (JNK) and NF-κB cascades are redox-sensitive signaling cascades that are capable of inducing the expression of proinflammatory cytokines and chemokines, e.g., TNF-α.[12] Among the NPs, only the UFPs were capable of JNK activation and TNF-α production (Figure 7 A,B and Figure S6B). This response was dose-dependent (Figure 6B). The UFPs that we used in this application contain a small amount (20 U/mL) of endotoxin (Table S2). Polymyxin B was used to rule out possible endotoxin effects on TNF-α production. Thus, while PMB was capable of a significant suppression of the LPS-induced response, it had a small effect on the UFP response (Figure S6C). None of the manufactured NPs contained any measurable (<0.1 U/mL) endotoxin levels (Table S2). This rules out the possibility that endotoxin contamination was responsible for this proinflammatory effect. Despite their ability to generate ROS, NH_2-PS nanospheres were ineffective inducers of JNK activation or cytokine production (Figure 7B). This supports the notion that these particles operate via different mechanisms.

To demonstrate the dynamic relationship between protective and proinflammatory cellular responses, the effect of increase of phase II enzyme expression was investigated on the UFP-induced responses (Figure 7C). Sulforaphane (SFN) is an electrophilic chemical that is capable of transcriptional activation of phase II gene promoters without inducing overt toxicity. Prior treatment of RAW 264.7 cells with SFN resulted in HO-1 expression and interference in TNF-α production (Figure 7C, insert). HO-1 is a representative phase II enzyme.[16,17] Subsequent addition of UFP led to a blunted TNF-α response (Figure 7C). NAC was also capable of interfering in UFP-induced TNF-α production for reasons discussed earlier on (Figure 7C).

(F) NP Increase Cellular and Mitochondrial Calcium (Ca^{2+}) Levels. Oxidative stress is capable of inducing changes in the intracellular free calcium concentration, $[Ca^{2+}]_i$, or could perturb Ca^{2+} compartmentalization, with the potential to lead to cellular toxicity.[36] Mitochondrial Ca^{2+} levels, $[Ca^{2+}]_m$, were followed by treating Rhod-2 stained cells with NPs (Figure 8A). UFP exposure induced a significant increase in Rhod-2 fluorescence starting at 4 h; this increase is progressive, culminating in a 2.5-fold increase by 16 h (Figure 8A). When repeated with manufactured NP, only the amino-modified PS nanospheres exerted a comparable (2-fold) effect; fullerol generated a smaller yet still statistically significant increase (Figure 8A,B). The intimate relationship of $[Ca^{2+}]_m$ and $[Ca^{2+}]_i$ was further demonstrated with Fluo-3 (Figure S7). Cellular staining with this dye

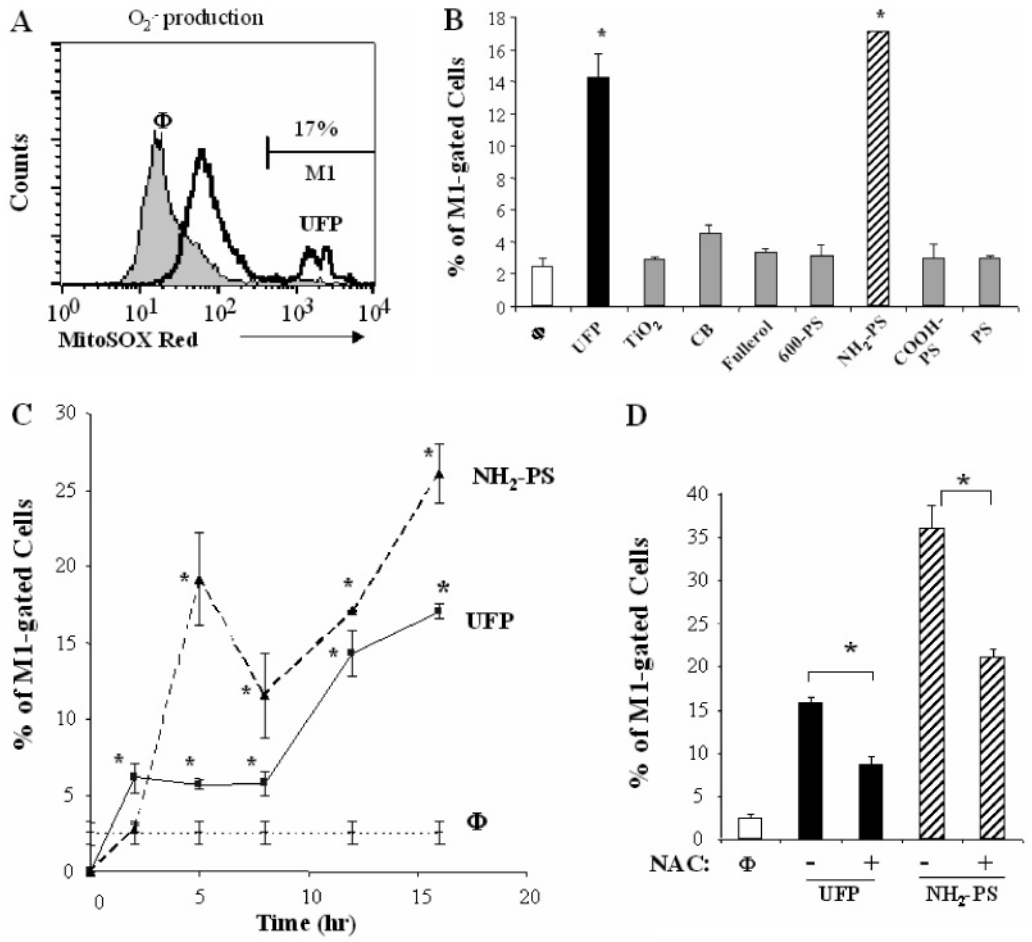

Figure 4. Mitochondrial $O_2^{\bullet -}$ production in RAW 264.7 cells after treatment with NP: (A) histogram to show the generation of a population of bright-positive (M1-gated) cells, obtained by staining of RAW 264.7 cells with MitoSOX Red (2 μM) and treatment with UFPs (10 μg/mL) for 12 h; (B) 12 h time point of MitoSOX Red-stained cells treated with a 10 μg/mL dose of UFPs, fullerol, CB, TiO_2, or PS particles. The flow data were expressed as a bar graph to show the percent of MitoSOX Red bright-positive cells; (C) time course of increased MitoSOX fluorescence in cells treated with 10 μg/mL UFP or NH_2-PS; (D) effect of NAC (10 mM) on cells treated with 10 μg/mL UFP or NH_2-PS for 16 h. Data are representative of three separate experiments. *$p < 0.01$, compared to control.

reflects $[Ca^{2+}]_i$, which was increased in response to UFP and NH_2-PS (Figure S7). All considered, these data demonstrate that particle-generated oxidative stress influence cellular and mitochondrial function via a Ca^{2+}-regulated pathway that has a recognized link to cytotoxicity.

(G) Electron Microscopy Reveals NP Uptake and Mitochondrial Damage. Detailed investigation of nanomaterial toxicity should consider NP uptake and subcellular localization. Mitochondria have been identified as a possible subcellular target for UFP, fullerene derivatives, and micellar nanocontainers.[19] Electron microscopy (EM) analysis of RAW 264.7 cells demonstrated mitochondrial swelling <4 h of the addition of UFP (data not shown). This was followed by loss of cristae and the appearance of intracellular vacuoles that contain electron dense material (Figure 9B). These changes were progressive, ultimately resulting in large particle-filled vacuoles and disappearance of mitochondria (Figure 9B). In contrast, TiO_2 particles were taken up into lose-fitting phagosomes without noticeable mitochondrial damage (Figure 9C). Similarly, CB particles were taken up in phagosomes without mitochondrial damage (not shown). Although it was difficult to visualize fullerol uptake, approximately 10% of the cells showed electron dense clumps that appear not to be membrane bound (Figure 9D). Mitochondria remained intact in >95% of these cells.

Anionic and cationic PS nanospheres were responsible for contrasting morphological changes. Carboxylated-NP was taken up in loose-fitting phagosomes, with preservation of mitochondria architecture. (Figure 9E). In contrast, NH_2−PS nanospheres could be seen to collect in large membrane-bound vacuoles and the nuclei of cells that showed disappearance of mitochondria (Figure 9F). This suggests that the cationic particles could enter an endocytic compartment that targets mitochondria, similar to UFP. Sixty nanometer PS particles and 600 nm NH_2-PS particles did not exhibit noticeable cellular uptake or damage (not shown).

(H) NP Exerts Functional Effects on Mitochondria and Induces Cellular Toxicity. Toxic oxidative stress can perturb mitochondrial function in a number of ways, including disruption of electron flow in the inner membrane, dissipation of the mitochondrial membrane potential ($\Delta\Psi$m), mitochondrial Ca^{2+} uptake, and large-scale opening of the PTP.[36] Using fluorescent dyes that are tracked in a flow cytometer, one can follow these changes. $DiOC_6$ is a cationic dye that

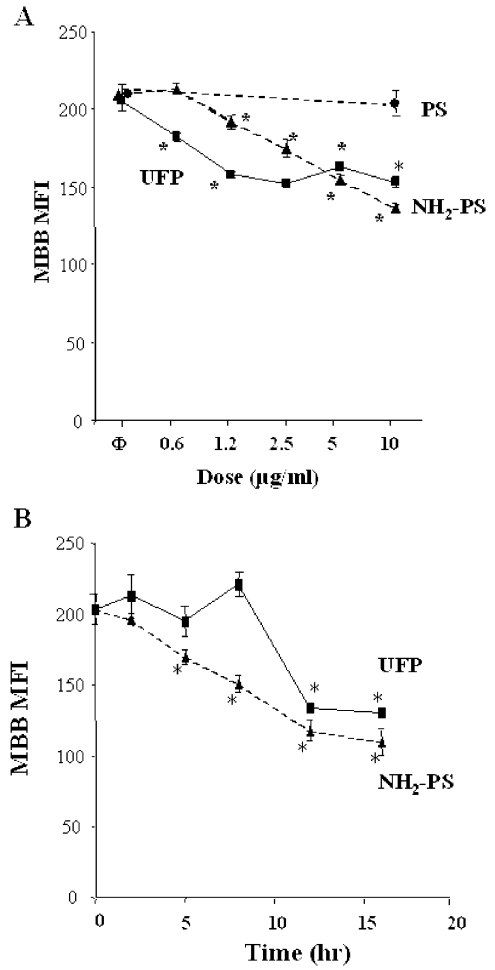

Figure 5. Decrease in intracellular thiol levels in response to NP treatment in RAW 264.7 cells: (A) histogram to display the decrease in MFI in MBB-stained (40 μM) RAW 264.7 cells, following treated with the indicated amount of the particles for 16 h; (B) time course of the change in MBB fluorescence in cells exposed to 10 μg/mL of the indicated particles. Data are representative of three separate experiments. *$p < 0.01$, compared to control.

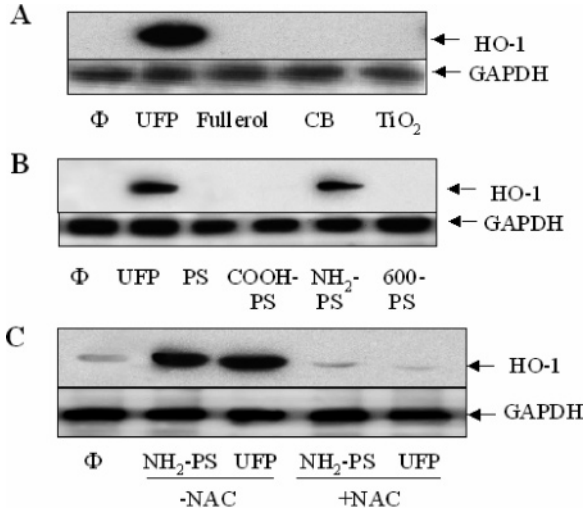

Figure 6. Induction of HO-1 expression, as determined by immunoblotting. RAW 264.7 cells were treated with 10 μg/mL of each individual NP for 16 h, before cellular extraction. (A) Comparison of the effects of UFP with fullerol, CB, and TiO_2. (B) Comparison of the effects of UFPs with PS nanospheres. (C) Effects of NAC (10 mM) on HO-1 expression. The lower panel in each blot shows equal protein loading as determined by GAPDH immunoblotting. Data are representative of two separate experiments.

is highly concentrated in the negatively charged mitochondrial matrix. Dissipation of the $\Delta\Psi$m leads to the $DiOC_6$ release and decreases cellular fluorescence as seen during treatment with UFP and NH_2-PS (Figure 10A). These changes commence within an hour of the addition of the UFPs but require a longer incubation period (>6 h) upon addition of NH_2-PS (not shown). Compared to the effects of UFPs and NH_2-PS, fullerol, CB, TiO_2, and other PS particles failed to exert an influence on the $\Delta\Psi$m (Figure 10B).

Large-scale PTP opening leads to mitochondrial depolarization, $O_2^{\bullet-}$ production and the release of pro-apoptotic factors.[37] Cellular toxicity was assessed by propidium iodide (PI) staining (Figure 10C). UFPs induced a dose-dependent increase in PI uptake in the nuclei of damaged cells; these changes commenced at a particle dose of 0.5 μg/mL (not shown). Compared to the statistically significant increase in PI fluorescence with UFPs, TiO_2, CB, and fullerol were inactive (Figure 10D). Among the PS particles, only the NH_2-nanospheres induced a significant increase in the % PI-positive cells (Figure 10D). NAC could interfere in the cytotoxicity of UFP and NH_2-PS (Figure 10E).

Discussion. In this study we looked at the adverse biological effects of ambient ultrafines in parallel with manufactured NPs. Our study was carried out in a phagocytic cell line that is representative of the macrophages and dendritic cells that are targeted by aerosolized nanoparticles in the lung.[38] Characterization of the particle physicochemical properties show a dramatic change in their state of aggregation, dispersibility, and charge during transfer from an aqueous solution to protein-containing tissue culture medium. NPs also differed with respect to cellular uptake, subcellular localization, and ability to catalyze ROS production under biotic and abiotic conditions. Ambient UFPs and cationic PS nanospheres were capable of ROS production, thiol depletion, and the induction of mitochondrial damage and cellular toxicity. Although an increase in TNF-α production could be seen in conjunction with mitochondrial damage and cytotoxicity during UFP exposure, NH_2-PS nanospheres induced mitochondrial damage and cytotoxicity without proinflammatory effects (Figure 7). These data show that assays for ROS production and oxidant injury provide a means of comparing the toxicity of a range of NPs. This investigation will now be extended to other nanomaterials to demonstrate the wider application of the approach.

The unique physicochemical properties of NPs are attributable to variables such as small size, large surface area, chemical composition, crystallinity, electronic properties, surface reactivity, inorganic/organic coatings, solubility, shape, and state of aggregation. Particles <100 nm fall in the transitional zone between individual molecules and bulk materials of the same composition. As the particle diameter approaches the nanoscale dimension, there is a dramatic

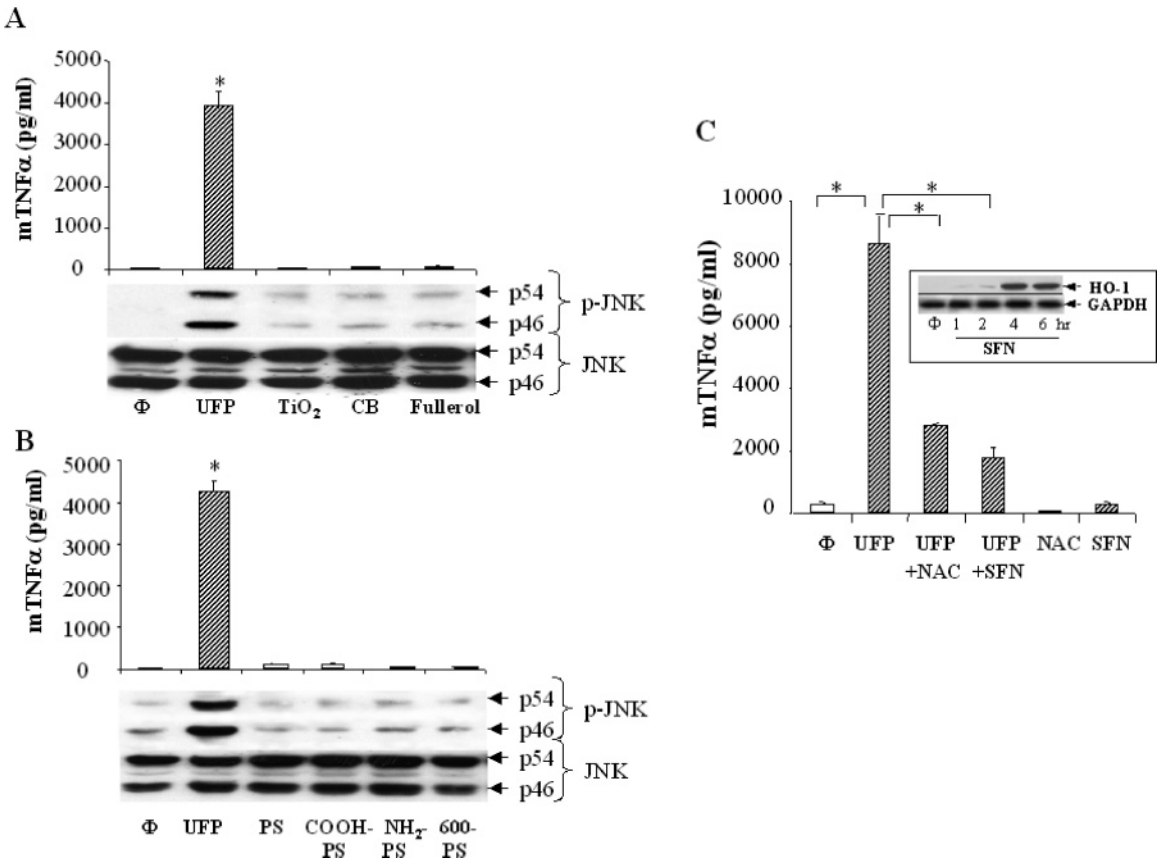

Figure 7. Jun kinase activation and TNF-α production in response to NPs. RAW 264.7 cells were treated with 10 μg/mL of each of the individual NP for 3 h before cellular extraction and anti-phosphopeptide and protein immunoblotting to reveal JNK activation. For enzyme-linked immunosorbent assay (ELISA), cells were incubated with 10 μg/mL of particles for 6 h, before harvesting of the supernatants for assessment of TNF-α levels by ELISA. (A) ELISA and immunoblotting results to compare UFP with fullerol, CB, and TiO_2. (B) Similar analysis for the comparison of UFP with PS nanospheres. (C) NAC (10 mM) and SFN (5 μm) were introduced to RAW 264.7 cells for 2 and 4 h, respectively, before the addition of 10 μg/mL UFPs for an additional 6 h. Supernatants were harvested to measure TNF-α levels by ELISA. The inserted immunoblot shows the effect of SFN on HO-1 expression. Data are representative of four separate experiments. *$p < 0.01$, compared to control.

increase in surface area and display of chemically reactive groups on the surface that could play a role in the adverse biological effects. For instance, a change in the material properties to create discontinuous crystal planes or enhance of electron storage can contribute to ROS generation. Alternatively, the increased surface reactivity could lead to protein denaturation, membrane damage, DNA cleavage, immune reactivity, and inflammation.[2] The small size of NP is also responsible for deep penetration in the lung where they have a high rate of retention due to van der Waals interactions.[39] Ultimately the effect of the small particle size combines with particle number and surface area to determine the actual dose of exposure, which could be more accurate than using a weight metric alone. Although we used weight/volume calculations for dispensing the particles into tissue culture medium, the difference in particle size and number could actually translate into differences in the total surface area, which could be a better measure of dose. Although it is possible to calculate the combined surface area of monodisperse particles by some straightforward methods, these calculations are inaccurate when the particles begin to aggregate, as seen in our study.

Previous studies on the toxicological effects of DEPs, which are emitted in the nanorange, demonstrated their ability to induce ROS, oxidative stress, and mitochondrial damage in target cells such as alveolar macrophages and bronchial epithelial cells.[19,40−43] Cellular studies have also demonstrated that organic DEP extracts induce protective and injurious cellular responses, including the expression of phase II enzymes, cytokine and chemokine production, and the initiation of programmed cell death.[15] These constitute the elements of the hierarchical oxidative stress response. We now extend those studies by demonstrating that UFPs induce similar effects. It is important to recognize that the protective and injurious cellular responses are in dynamic equilibrium and that weakening or strengthening of the phase II response could determine susceptibility to oxidant injury. This principle is illustrated by the use of SFN, a nontoxic chemical that induces a phase II response in RAW 264.7 cells (Figure 7C). Subsequent UFP exposure protects these cells from proinflammatory and cytotoxic effects (Figure 7C).

The use of the oxidative stress paradigm to study the effects of manufactured NPs lead to a number of interesting and novel observations. While NH_2-PS nanospheres are capable of cellular ROS production and induction of oxidant

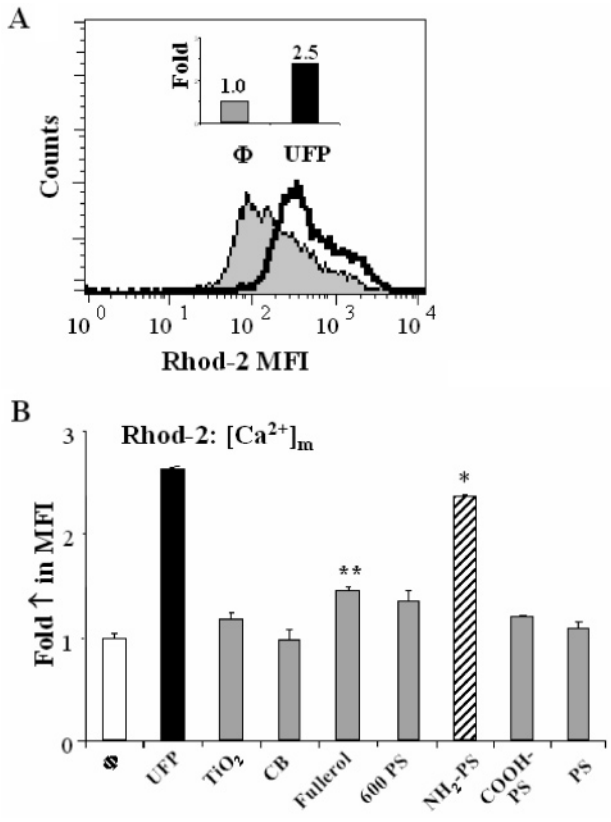

Figure 8. Effect of NPs on mitochondial calcium levels, $[Ca^{2+}]_m$: (A) histogram showing the fold-increase in MFI in RAW 264.7 cells, which were incubated with 4 μM Rhod-2 for 0.5 h after the addition of 10 μg/mL UFP for an 16 h; (B) comparison of the MFI of cells treated with 10 μg/mL UFPs, fullerol, CB, TiO_2, and PS nanospheres for 16 h. Data are representative of three separate experiments. *$p < 0.01$ or **$p < 0.05$, compared to control.

stress injury, other NPs were incapable of doing the same (Figures 3−5). While fullerol was capable of producing small amounts of H_2O_2 in conjunction with a small increase in $[Ca^{2+}]_m$, there was no increase in cellular toxicity (Figure 8). This suggests a subthreshold effect or suppression of injurious effects by an effective antioxidant defense mechanism. However, we found no evidence that fullerol could induce HO-1 expression (Figure 6). Despite the lack of spontaneous ROS production, cationic PS nanospheres were as toxic as ambient UFP (Figures 8 and 10). Different from UFPs, however, NH_2-PS nanospheres did not induce JNK activation or TNF-α production, suggesting a different mechanism of action (Figure 7).

Comparison of ROS production under biotic or abiotic conditions yielded different response profiles. In one example, TiO_2 and fullerol were capable of ROS generation in a cell-free system but incapable of doing so in RAW 264.7 cells, despite effective particle uptake (Figures 2 and 9). This outcome is diagonally opposite from the effects of cationic PS nanospheres, which were capable of cellular H_2O_2 and $O_2^{\bullet-}$ production but incapable of doing so under abiotic conditions (Figures 2−4). In contrast, UFPs generate ROS under biological and nonbiological conditions, while CB and carboxylated-PS particles are inactive in both environments (Figures 2−4). These differences are the result of differences in material composition, size, and charge.

We have previously demonstrated that redox-cycling of organic chemicals and transition metals play an important role in particle-induced ROS generation.[19,21] This includes H_2O_2 production, which likely originates from $O_2^{\bullet-}$ through spontaneous or enzyme-catalyzed dismutation. Functionalized organic chemical groups, such as oxy-PAH and quinones, are capable of $O_2^{\bullet-}$ generation by redox cycling reactions that involve an intermediary electron acceptor (e.g., semiquinones). Enzyme-assisted one-electron transfers, e.g., microsomal NADPH−P450 reductase, can strengthen this reaction in cells.[44] The presence of transition metals assists in the formation of additional radicals, e.g., the hydroxyl radical ($OH^{\bullet}$), through the catalysis of the Fenton reaction. Mitochondrial perturbation represents another source of UFP-induced ROS generation. This involves interference in inner membrane electron transfer, mitochondrial depolarization, and opening of the PTP in response to PM chemicals.[20] From a kinetic perspective, it is noteworthy that H_2O_2 generation by UFP commences early and then declines >4 h, while $O_2^{\bullet-}$ production starts later and is progressive in nature (Figures 3 and 4C). We propose that these different phases of ROS production represent different mechanisms. One possibility is that the early phase of ROS production is due to redox cycling chemistry, while mitochondria are responsible for the late and progressive increase in $O_2^{\bullet-}$. In contrast to ambient UFPs, CB particles contain small quantities of redox cycling chemicals and are incapable of ROS generation (Table S1). In accordance with this notion, CB was inert in our biological assays.

ROS generation by TiO_2 occurs when absorbed photons promote electrons across the TiO_2 band gap to the conduction band, simultaneously creating a vacancy or hole in the valence band of the semiconductor.[45] Electrons that diffuse to the surface may react with oxygen to form the $O_2^{\bullet-}$. Electron holes that diffuse to the surface may react with adsorbed water to form hydroxyl radicals.[45] TiO_2 does not form these highly reactive species in the dark. The rutile form of TiO_2 absorbs light over a slightly broader range of wavelengths than does the anatase form. However, it is the anatase form that exhibits a higher photocatalytic activity. In contrast to their ability to generate ROS under illuminated abiotic conditions, TiO_2 nanoparticles are incapable of doing so in RAW 264.7 cells (Figures 3 and 4).[46] Although ROS production has been described in pulmonary alveolar macrophages, exposure to TiO_2 nanoparticles was not associated with lung damage.[47,48] Although the explanation provided for this dichotomy was the induction of an adaptive response,[47,48] we found no evidence that TiO_2 is capable of phase II enzyme expression (Figure 6). This could mean that passivation of the NP surface by culture medium components could prevent ROS production or otherwise that any ROS that are produced in the cell could be easily neutralized by available antioxidant defense mechanisms.

ROS production by fullerol occurs via two pathways. In the first, a photon can excite fullerol from the ground to a singlet state, where it has a nanosecond lifetime. Singlet state

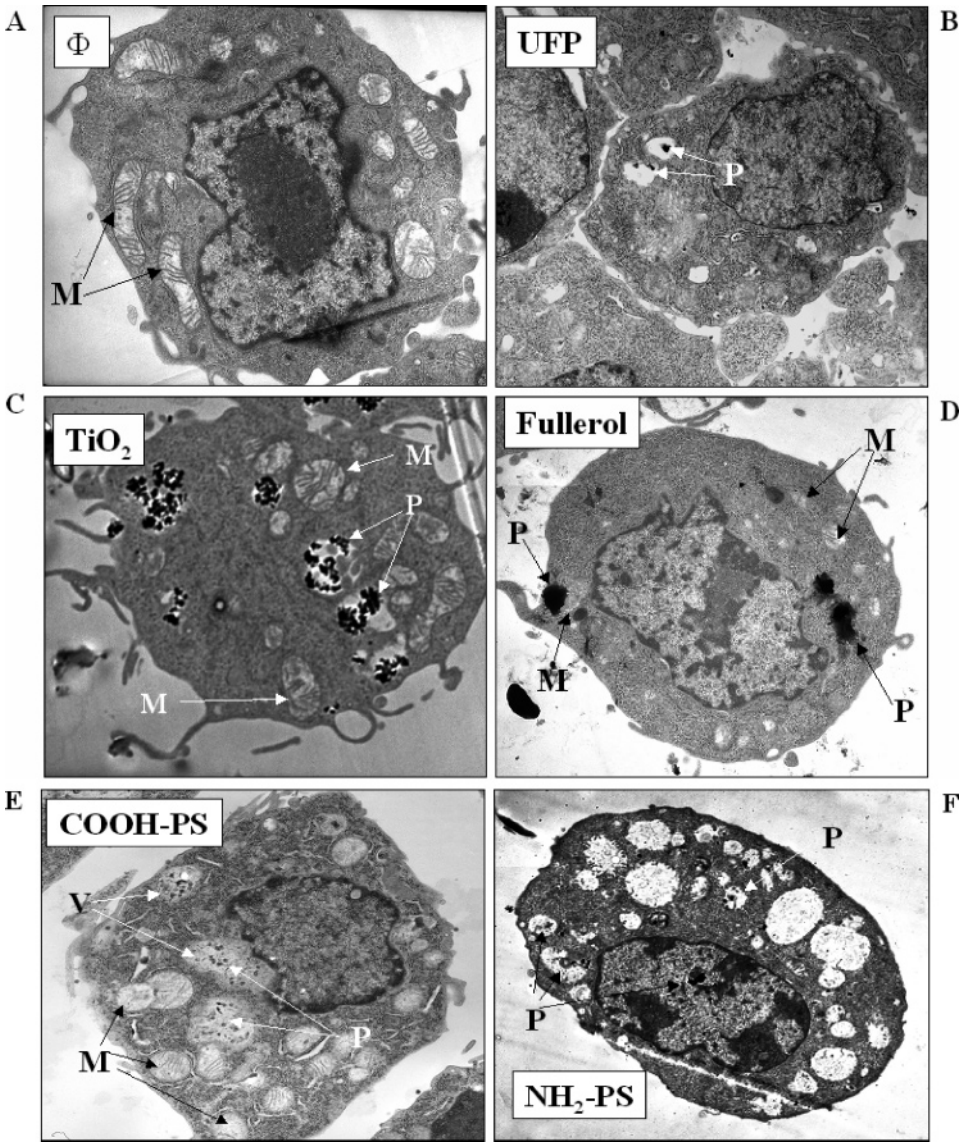

Figure 9. Use of electron microscopy to determine the uptake and subcellular localization of NP. The procedure is described in the Supporting Information. (A) Untreated RAW 264.7 cells. (B) Cells were treated with 10 μg/mL UFPs for 16 h. Similar analysis conditions for: (C) TiO_2, (D) fullerol, (E) COOH-PS nanospheres, and (F) NH_2-PS nanospheres. Labels: M = mitochondria, P = particles.

fullerol may then relax to the longer-lived triplet state where it readily reacts with ground-state oxygen to form singlet oxygen via what is known as a type I pathway.[27,30] The triplet state fullerol can also be reduced by appropriate electron donors and subsequently oxidized by oxygen to form $O_2^{\bullet-}$ via the type II pathway. Alternatively, in the absence of light and in the appropriate redox conditions, fullerol may act as an electron shuttle between electron donors and oxygen to form $O_2^{\bullet-}$.[27] Our observations of ROS production by fullerol in this and previous studies[28,49,50] appear to contradict conclusions from another study that explained low grade fullerol toxicity as being due to a lack of ROS production.[51] Indeed, fullerol was observed in the current study to induce spontaneous as well as cellular ROS production (Figures 2 and 3). The increase in cellular H_2O_2 production was associated with a modest increase in the $[Ca^{2+}]_m$, but did not induce cytotoxicity, likely due to a failure to release pro-apoptotic factors from the mitochondria.

Although capable of ROS generation and cellular toxicity, cationic PS nanospheres differ in their action from ambient UFP. This includes lack of spontaneous ROS generation, different kinetics of the cellular ROS response, and a failure to induce TNF-α production (Figures 2−4 and 7). Although we lack an exact explanation for the sequence of events that follow the introduction of NH_2-PS nanospheres, it has been suggested previously that positively charged polyamine-coated PS microparticles engage in strong ionic interactions with the negatively charged cell membrane.[52,53] The strength of these interactions facilitates particle uptake into tight-fitting phagosomes, compared to the more loose-fitting phagosomes that forms around negatively charged particles. Tight adherence of the cationic particles to the membrane interferes in phagosomal fusion with lysosomes. As a result, these phagosomes become isolated in the cytoplasm, with the possibility that the particles could escape to the cytosol after endosomal rupture.[52,53] Behr proposed the so-called

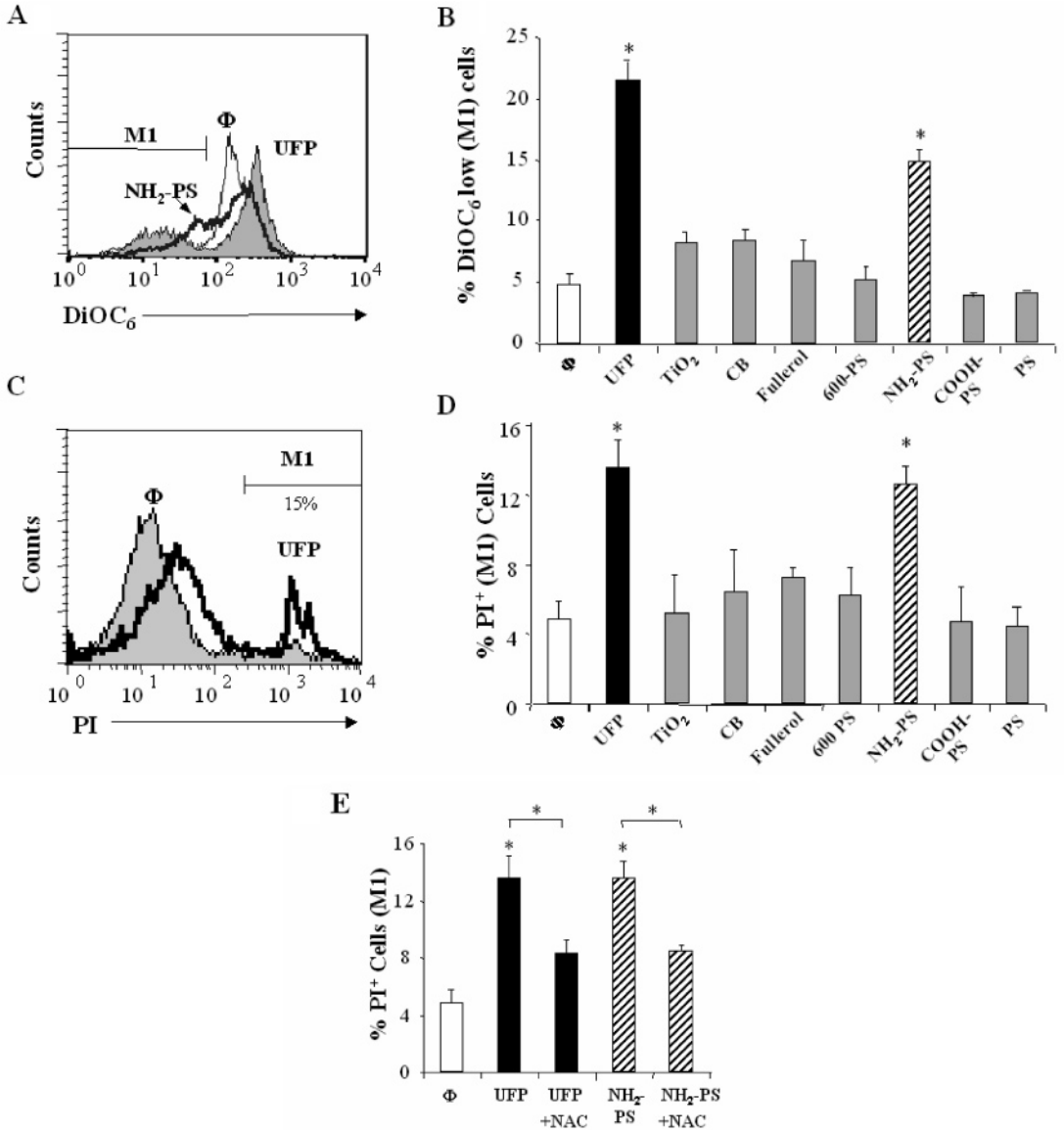

Figure 10. Changes in mitochondrial membrane potential ($\Delta\Psi$m) and cellular toxicity (PI uptake) during NP exposure. Cells were treated with UFP or manufactured NP for 16 h before staining with 20 nM $DiOC_6$. (A) Histogram to show the decrease in $DiOC_6$ fluorescence in response to UFP treatment; this decrease represents a decline in $\Delta\Psi$m. The M1 bar was used to score the percent of $DiOC_6^{lo}$ cells. (B) Comparison of the percent of $DiOC_6^{lo}$ cells 16 h following the addition of 10 μg/mL UFPs, fullerol, CB, TiO_2, or PS nanospheres. (C) Histogram to show PI uptake in RAW 264.7 cells treated with 10 μg/mL UFPs for 16 h. M1 gating was used to assess the percent PI^+ cells, which represent cells that are extensively damaged. (D) PI^+ cells after treatment with UFPs, fullerol, CB, TiO_2, and PS nanospheres for 16 h. (D) Effect of NAC (10 mM) on cytotoxicity by UFPs and 60 nm NH_2-PS particles. Data are representative of three separate experiments. *$p < 0.01$, NAC treated versus non-NAC treated samples.

proton sponge hypothesis to explain the mechanism of rupture.[54] His theory posits that extensive buffering by the cationic particle surface may lead to unchecked proton transport into the phagosome. This could lead to excessive water influx, which, due to the space constraints, leads to endosome rupture. From there, the particles may engage other membrane-protected spaces, such as mitochondria. The above sequence of events may explain the formation of particle-filled vacuoles and the disappearance of mitochondria from the cell (Figure 9). Mitochondrial damage may contribute to the late phase of $O_2^{\bullet-}$ production (Figures 4C and 9). Although the origin is of the first wave of ROS production is uncertain, it is possible that NH_2-PS could induce the assembly and activation of NADPH oxidase; this enzyme is responsible for $O_2^{\bullet-}$ production in the phagosomal membrane. It is also interesting that while the first wave of $O_2^{\bullet-}$ generation is insensitive to NAC quenching, this antioxidant could suppress the second wave of NH_2-PS-induced $O_2^{\bullet-}$ generation (Figure 4C). NAC is capable of suppressing $O_2^{\bullet-}$ production in mitochondria from cells undergoing apoptosis (Figure 10E).[41]

All considered, ambient UFPs and NH_2-PS nanoparticles showed the clearest evidence of toxicity and stand apart from the other particle types, even particles capable of spontaneous ROS production (TiO_2 and fullerol). We would therefore rank UFPs and NH_2-PS nanospheres as the most toxic, with ambient UFPs having the additional effect of inducing proinflammatory responses. Among the nontoxic particles,

fullerol was the only material that could elicit significant ROS production along with a small increase in $[Ca^{2+}]_m$. It is possible, therefore, to distinguish potentially toxic from nontoxic particles and to interpret the range of cellular responses in terms of the hierarchical oxidative stress paradigm, which includes protective and injurious effects.

Our study did not address NP effects on other cell types that could be relevant to particle toxicity. This includes cells at the portal-of-entry toxicity sites such as bronchial epithelial cells and keratinocytes, as well as cells that are targeted after particle uptake and spread in the body such as hepatocytes, kidney cells, endothelial cells, neurons, etc. We are in the process of applying our methodology to the study of these cell types, with preliminary data suggesting response differences due to differences in cellular uptake, subcellular localization, and engagement of biological pathways leading to ROS production. Moreover, we also aim to use animal experimentation to see if these experimental principles apply to in vivo injury and pathogenesis of disease as demonstrated by animal exposures to PM.

In summary, we have demonstrated that ROS generation and oxidative stress can be used as a paradigm to assess NP toxicity. Although not all NPs exhibit the electronic configurations or surface properties that allow spontaneous ROS generation, particle interactions with cellular components could generate ROS during these interactions. This could lead to cellular toxicity if the magnitude of ROS production overwhelms the antioxidant defense of the cell or induce mitochondrial apoptotic mechanisms. The assessment of ROS production and generation of oxidative stress is a valid mechanism of comparing the toxicity of manufactured or ambient NPs.

Acknowledgment. Funding for this study was provided by the US Public Health Service Grants, U19 A1070453, RO1 ES10553, RO1 ES10253, RO1 ES015498, and RO1 ES13432, as well as the U.S. EPA STAR award (RD-83241301) to the Southern California Particle Center. Nanobiosensor work was funded by NIH (GM/AI66466, J.I.Y.), AFSOR/MURI (F49620-03-1-0365, J.I.Y.) to Joanne I. Yeh. This research was also supported in part by the use of resources and facilities of the William S. Middleton Veterans Administration Hospital, Madison, WI. This work has not been subjected to the EPA for peer and policy review.

Supporting Information Available: Text describing detailed description of the materials and methods used and chemical characterization of the nanoparticles used, figures showing size distribution of particles and model of the bioassembly, and tables providing the characteristics of the nanoparticles and endotoxin content. This material is available free of charge via the Internet at http://pubs.acs.org.

References

(1) Donaldson, K.; Stone, V.; Clouter, A.; Renwick, L.; MacNee, W. *Occup. Environ. Med.* **2001**, *58*, 211−216.
(2) Nel, A.; Xia, T.; Madler, L.; Li, N. *Science* **2006**, *311*, 622−627.
(3) Oberdorster, G.; Oberdorster, E.; Oberdorster, J. *Environ. Health Perspect.* **2005**, *113*, 823−839.
(4) The Royal Society and Royal Academy of Engineerings, Nanoscience and nanotechnologies: Opportunities and uncertainties. 2004.
(5) Donaldson, K.; Stone, V.; Tran, C. L.; Kreyling, W.; Borm, P. J. *Occup. Environ. Med.* **2004**, *61*, 727−728.
(6) Donaldson, K.; Tran, C. L. *Inhalation Toxicol.* **2002**, *14*, 5−27.
(7) Nel, A. *Science* **2005**, *308*, 804−806.
(8) Oberdorster, E. *Environ. Health Perspect.* **2004**, *112*, 1058−1062.
(9) Monteiro-Riviere, N. A.; Nemanich, R. J.; Inman, A. O.; Wang, Y. Y.; Riviere, J. E. *Toxicol. Lett.* **2005**, *155*, 377−384.
(10) Shvedova, A. A.; Castranova, V.; Kisin, E. R.; Schwegler-Berry, D.; Murray, A. R.; Gandelsman, V. Z.; Maynard, A.; Baron, P. J. *Toxicol. Environ. Health A* **2003**, *66*, 1909−1926.
(11) Shvedova, A. A.; Kisin, E. R.; Mercer, R.; Murray, A. R.; Johnson, V. J.; Potapovich, A. I.; Tyurina, Y. Y.; Gorelik, O.; Arepalli, S.; Schwegler-Berry, D.; Hubbs, A. F.; Antonini, J.; Evans, D. E.; Ku, B. K.; Ramsey, D.; Maynard, A.; Kagan, V. E.; Castranova, V.; Baron, P. *Am. J. Physiol.*: *Lung Cell. Mol. Physiol.* **2005**, *289*, L698−708.
(12) Warheit, D. B.; Laurence, B. R.; Reed, K. L.; Roach, D. H.; Reynolds, G. A.; Webb, T. R. *Toxicol. Sci.* **2004**, *77*, 117−125.
(13) Halliwell, B.; Gutteridge, J. M. C. *Free Radicals in Biology and Medicine*, 3rd ed.; Oxford University Press: Oxford, 1999; pp 246−350.
(14) Bell, A. T. *Science* **2003**, *299*, 1688−1691.
(15) Xiao, G. G.; Wang, M.; Li, N.; Loo, J. A.; Nel, A. E. *J. Biol. Chem.* **2003**, *278*, 50781−50790.
(16) Chan, K.; Kan, Y. W. *Proc. Natl. Acad. Sci. U.S.A.* **1999**, *96*, 12731−12736.
(17) Li, N.; Alam, J.; Venkatesan, M. I.; Eiguren-Fernandez, A.; Schmitz, D.; Di, S. E.; Slaughter, N.; Killeen, E.; Wang, X.; Huang, A.; Wang, M.; Miguel, A. H.; Cho, A.; Sioutas, C.; Nel, A. E. *J. Immunol.* **2004**, *173*, 3467−3481.
(18) Donaldson, K.; Stone, V.; Borm, P. J.; Jimenez, L. A.; Gilmour, P. S.; Schins, R. P.; Knaapen, A. M.; Rahman, I.; Faux, S. P.; Brown, D. M.; MacNee, W. *Free Radicals Biol. Med.* **2003**, *34*, 1369−1382.
(19) Li, N.; Sioutas, C.; Cho, A.; Schmitz, D.; Misra, C.; Sempf, J.; Wang, M.; Oberley, T.; Froines, J.; Nel, A. *Environ. Health Perspect.* **2003**, *111*, 455−460.
(20) Xia, T.; Korge, P.; Weiss, J. N.; Li, N.; Venkatesen, M. I.; Sioutas, C.; Nel, A. *Environ. Health Perspect.* **2004**, *112*, 1347−1358.
(21) Geller, M. D.; Kim, S.; Misra, C.; Sioutas, C.; Olson, B. A.; Marple, V. A. *Aerosol Sci. Technol.* **2002**, *36*, 748−762.
(22) Burtscher, H. J. *Aerosol Sci.* **2005**, *36*, 896−932.
(23) Park, K.; Kittelson, D. B.; McMurry, P. H. *Aerosol Sci. Technol.* **2004**, *38*, 881−889.
(24) Nel, A. E.; Diaz-Sanchez, D.; Li, N. *Curr. Opin. Pulm. Med.* **2001**, *7*, 20−26.
(25) Borm, P. J.; Cakmak, G.; Jermann, E.; Weishaupt, C.; Kempers, P.; van Schooten, F. J.; Oberdorster, G.; Schins, R. P. *Toxicol. Appl. Pharmacol.* **2005**, *205*, 157−167.
(26) Hohr, D.; Steinfartz, Y.; Schins, R. P.; Knaapen, A. M.; Martra, G.; Fubini, B.; Borm, P. J. *Int. J Hyg. Environ. Health* **2002**, *205*, 239−244.
(27) Mohan, H.; Palit, D.; Mittal, J.; Chiang, L. Y.; Asmus, K.; Guldi, D. M. *Faraday Trans.s* **1998**, *94*, 359−363.
(28) Pickering, K.; Wiesner, M. *Environ. Sci. Technol.* **2005**, *39*, 1359−1365.
(29) Guldi, D.; Prato, M. *Acc. Chem. Res.* **2000**, *33*, 695−703.
(30) Prat, F.; Stackow, R.; Bernstein, R.; Qian, W.; Rubin, Y.; Foote, C. S. *J. Phys. Chem. A* **1999**, *103*, 7230−7235.
(31) Sotiropoulou, S.; Chaniotakis, N. A. *Anal. Bioanal. Chem.* **2003**, *375*, 103−105.
(32) Guiseppi-Elie, A.; Lei, C.; Baughman, R. H. *Nanotechnology* **2002**, *13*, 559−564.
(33) Cai, C.; Chen, J. *Anal. Biochem.* **2004**, 332, 75−83.
(34) Kleiner, H. E.; Rivera, M. I.; Pumford, N. R.; Monks, T. J.; Lau, S. S. *Chem. Res. Toxicol.* **1998**, *11*, 1283−1290.
(35) Julian, D.; April, K. L.; Patel, S.; Stein, J. R.; Wohlgemuth, S. E. *J. Exp. Biol.* **2005**, *208*, 4109−4122.
(36) Brookes, P. S.; Yoon, Y.; Robotham, J. L.; Anders, M. W.; Sheu, S. S. *Am. J. Physiol.*: *Cell Physiol.* **2004**, *287*, C817−C833.
(37) Green, D. R.; Kroemer, G. *Science* **2004**, *305*, 626−629.
(38) Chan, R. C.; Wang, M. Y.; Li, N.; Yanagawa, Y.; Onoe, K.; Lee, J. J.; Nel, A. J *Allergy Clin. Immunol.* **2006**, *118*, 455−465.
(39) Pietropaoli, A. P.; Frampton, M. W.; Hyde, R. W.; Morrow, P. E.; Oberdorster, G.; Cox, C.; Speers, D. M.; Frasier, L. M.; Chalupa, D. C.; Huang, L. S.; Utell, M. J. *Inhalation Toxicol.* **2004**, *16* Suppl 1, 59−72.

(40) Hiura, T. S.; Kaszubowski, M. P.; Li, N.; Nel, A. E. *J. Immunol.* **1999**, *163*, 5582−5591.
(41) Hiura, T. S.; Li, N.; Kaplan, R.; Horwitz, M.; Seagrave, J. C.; Nel, A. E. *J. Immunol.* **2000**, *165*, 2703−2711.
(42) Li, N.; Venkatesan, M. I.; Miguel, A.; Kaplan, R.; Gujuluva, C.; Alam, J.; Nel, A. *J. Immunol.* **2000**, *165*, 3393−3401.
(43) Li, N.; Wang, M.; Oberley, T. D.; Sempf, J. M.; Nel, A. E. *J. Immunol.* **2002**, *169*, 4531−4541.
(44) Sagai, M.; Saito, H.; Ichinose, T.; Kodama, M.; Mory, M. *Free Radical Biol. Med.* **1993**, *14*, 37−47.
(45) Hoffmann, M. R.; Martin, S. T.; Choi, W.; Bahnemann, D. W. *Chem. Rev.* **1995**, *95*, 69−96.
(46) Chauhan, V.; Breznan, D.; Goegan, P.; Nadeau, D.; Karthikeyan, S.; Brook, J. R.; Vincent, R. *Cell Biol. Toxicol.* **2004**, *20*, 221−239.
(47) Olmedo, D. G.; Tasat, D. R.; Guglielmotti, M. B.; Cabrini, R. L. *J Biomed. Mater. Res., Part A* **2005**, *73*, 142−149.
(48) Dick, C. A.; Brown, D. M.; Donaldson, K.; Stone, V. *Inhalation Toxicol.* **2003**, *15*, 39−52.
(49) Vileno, B.; Lekka, M.; Sienkiewicz, A.; Marcoux, P.; Kulik, A. J.; Kasas, S.; Catsicas, S.; Graczyk, A. *J. Phys.*: *Condens. Matter* **2005**, *17*, S1471−S1482.
(50) Vileno, B.; Marcoux, P.; Lekka, M.; Sienkiewicz, A.; Feher, T.; Forro, L. *Adv. Funct. Mater.* **2006**, *16*, 120−128.
(51) Sayes, C.; Fortner, J.; Lyon, D.; Boyd, A.; Ausman, K.; Guoh, W.; Tao, Y.; Sitharaman, B.; Wilson, L.; West, J.; Colvin, V. *Nano Lett.* **2004**, *4*, 1881−1887.
(52) Oh, Y. K.; Swanson, J. A. *J. Cell Biol.* **1996**, *132*, 585−593.
(53) Foged, C.; Brodin, B.; Frokjaer, S.; Sundblad, A. *Int. J. Pharm.* **2005**, *298*, 315−322.
(54) Boussif, O.; Lezoualc′h, F.; Zanta, M. A.; Mergny, M. D.; Scherman, D.; Demeneix, B.; Behr, J. P. *Proc. Natl. Acad. Sci. U.S.A.* **1995**, *92*, 7297−7301.

NL061025K